Aven-mediated checkpoint kinase control regulates proliferation and resistance to chemotherapy in conventional osteosarcoma

Baranski, Z.; Booij, T.H.; Cleton-Jansen, A.M.; Price, L.S.; Water, B. van de; Bovee, J.V.M.G.; ... ; Danen, E.H.J.

Journal of Pathology
J Pathol 2015; **236:** 348–359
Published online 30 March 2015 in Wiley Online Library (wileyonlinelibrary.com) DOI: 10.1002/path.4528

ORIGINAL PAPER

Aven-mediated checkpoint kinase control regulates proliferation and resistance to chemotherapy in conventional osteosarcoma

Zuzanna Baranski,[1] Tijmen H Booij,[1] Anne-Marie Cleton-Jansen,[2] Leo S Price,[1,3] Bob van de Water,[1] Judith VMG Bovée,[2] Pancras CW Hogendoorn[2]* and Erik HJ Danen[1]*

[1] *Division of Toxicology, Leiden Academic Centre for Drug Research, Leiden University, The Netherlands*
[2] *Department of Pathology, Leiden University Medical Centre (LUMC), The Netherlands*
[3] *OcellO B.V. Leiden, The Netherlands*

**Correspondence to: PCW Hogendoorn, Department of Pathology, Leiden University Medical Centre, PO Box 9600, 2300 RC Leiden, The Netherlands. E-mail: p.c.w.hogendoorn@lumc.nl*
Or EHJ Danen, Division of Toxicology, Leiden Academic Centre for Drug Research, Einsteinweg 55, 233CC Leiden, The Netherlands. E-mail: e.danen@lacdr.leidenuniv.nl

Abstract

Conventional high-grade osteosarcoma is the most common primary bone sarcoma, with relatively high incidence in young people. In this study we found that expression of Aven correlates inversely with metastasis-free survival in osteosarcoma patients and is increased in metastases compared to primary tumours. Aven is an adaptor protein that has been implicated in anti-apoptotic signalling and serves as an oncoprotein in acute lymphoblastic leukaemia. In osteosarcoma cells, silencing Aven triggered G_2 cell-cycle arrest; Chk1 protein levels were attenuated and ATR–Chk1 DNA damage response signalling in response to chemotherapy was abolished in Aven-depleted osteosarcoma cells, while ATM, Chk2 and p53 activation remained intact. Osteosarcoma is notoriously difficult to treat with standard chemotherapy, and we examined whether pharmacological inhibition of the Aven-controlled ATR–Chk1 response could sensitize osteosarcoma cells to genotoxic compounds. Indeed, pharmacological inhibitors targeting Chk1/Chk2 or those selective for Chk1 synergized with standard chemotherapy in 2D cultures. Likewise, in 3D extracellular matrix-embedded cultures, Chk1 inhibition led to effective sensitization to chemotherapy. Together, these findings implicate Aven in ATR–Chk1 signalling and point towards Chk1 inhibition as a strategy to sensitize human osteosarcomas to chemotherapy.

Keywords: osteosarcoma; Aven; Chk1 inhibitors; doxorubicin; 3D cell culture

Received 25 December 2014; Revised 23 February 2015; Accepted 4 March 2015

No conflicts of interest were declared.

Introduction

Osteosarcoma is the most common primary malignant bone tumour, occurring predominantly in children and adolescents and with a second peak at middle age. It is thought to arise from mesenchymal stem cells that are capable of producing osteoid [1,2]. At the time of diagnosis, 10–20% of patients present with metastasis. About 30–40% of patients with localized osteosarcoma will relapse, mainly by developing lung metastasis. Patients with recurrence have a very poor prognosis, with 23–33% 5-year overall survival [3].

Aven is an adaptor protein that exerts anti-apoptotic activity by potentiating Bcl–xL and by interfering with the self-association of Apaf-1, thereby preventing the activation of caspase 9 [4,5]. Aven has also been identified through bioinformatics analysis as a novel potential BH3 domain-containing protein [6]. Besides being involved in apoptosis, Aven was reported to control the DNA damage response (DDR) by physically interacting with, and supporting the activity of, 'ataxia–telangiectasia mutated' (ATM) [7].

The DDR is evolutionarily conserved and essential to ensure the faithful maintenance and replication of the genome. This elaborate integrated signalling cascade senses DNA damage and triggers repair, cell cycle arrest and, in the case of severe damage, cell death. The serine/threonine protein kinases of the phosphatidylinositol 3-kinase-like family, ATM and 'ATM and Rad3-related' (ATR), are crucial players in the DDR [8,9]. After DNA damage, ATM and ATR are activated and, in turn, activate critical effectors, including components of the DNA damage-repair machinery and the checkpoint kinases Chk1 and Chk2 to arrest the cell cycle [10]. Combining cytotoxic chemotherapeutics with pharmacological Chk1/Chk2 inhibitors can prevent damaged cancer cells from arresting, causing increased tumour cell killing and thus improved therapeutic efficacy [11].

In the context of cancer, Aven has thus far been exclusively implicated in haematopoietic malignancies. *Aven*

mRNA levels have been associated with disease relapse and poor prognosis of acute lymphoblastic leukaemia, and Aven has been shown to act as an oncoprotein that drives proliferation and survival of leukaemic cells [12–14]. Here, we analyse *Aven* mRNA, protein expression and function in osteosarcoma, the most common primary bone malignancy, which is very difficult to treat. We show that Aven expression is increased in metastatic lesions and inversely correlated with metastasis-free survival in osteosarcoma patients. We show that Aven is in fact dispensable for ATM–Chk2 (and p53) activation. Instead, Aven is required for ATR–Chk1 signalling and Aven silencing leads to G_2 cell cycle arrest. Moreover, in the absence of Aven, osteosarcoma cells fail to activate Chk1 (but not Chk2) in response to DNA-damaging chemotherapeutics. Finally, we show that targeting Aven-controlled ATR–Chk1 activity using clinically relevant pharmacological inhibitors sensitizes osteosarcoma to chemotherapy.

Materials and methods

Reagents and antibodies

Doxorubicin was obtained from the Department of Clinical Pharmacology at LUMC. AZD7762 Chk1/Chk2 inhibitor, Ly2603618 and CHIR-124 Chk1 inhibitors were from SelleckChem (Huissen, The Netherlands). Cisplatin and etoposide were from Sigma-Aldrich (Zwijndrecht, The Netherlands). Hoechst 33342 was from Fischer Scientific (Bleiswijk, The Netherlands) and the pan-caspase inhibitor z-VAD-fmk was from Bachem (WeilamRhein, Germany). The Aven antibody (HPA020 563) used for immunohistochemistry and antibody against tubulin (T-9026) was from Sigma-Aldrich (Zwijndrecht, The Netherlands). The Aven antibody (2300S) used for western blot and antibodies against phospho-ATR(Ser428) (2853), phospho-H3(ser10) (9701), phospho-CHK2(Thr68) (2661P), phospho-H2Ax(Ser 139) (9718), phospho-ATM(Ser1981) (5883), and CHK1 (2345) were from Cell Signaling (Bioké, Leiden, The Netherlands). The antibody against phospho-CHK1(Ser317; A300-163A) was from Bethyl Laboratories (Uithoorn, The Netherlands).

Microarray data analysis

Gene expression profiles were obtained from a previously published microarray dataset [15]. Using the Bioconductor lumi package, data had been transformed with the variance stabilizing transformation algorithm and normalized with the robust spline normalization algorithm. Probe_ID identifiers from the Illumina Annotation for Illumina human 6 v. 2.0 expression beadchip were used as reporters (Aven reporter = ILMN_1710216). Kaplan–Meier curves were created from the entry 'Mixed Osteosarcoma-Kuijer-127-vst-ilmnhwg6v2' in the web application R2 (http://r2.amc.nl).

Immunohistochemistry on tissue microarrays

Tissue microarrays used in this study were previously constructed and published [16]. All specimens in this study were handled according to the ethical guidelines described in *Code for Proper Secondary Use of Human Tissue in The Netherlands* of the Dutch Federation of Medical Scientific Societies. Slides were deparaffinized and rehydrated and endogenous peroxidase blocked. Subsequently, antigen retrieval was performed with citrate, pH 6.0. Incubation with antibody was overnight at 4 °C at a 1:1000 dilution. As a second step, we used Immunologic Poly-HRP-GAM/R/R IgG (DVPO110HRP) and Dako liquid DAB+ Substrate Chromogen System (K3468), after which the slides were counterstained with haematoxylin. Testis tissue was used as a control (see supplementary material, Figure S1). Slides were scored independently by two observers (JVMGB and ZB). Staining intensity (0, absent; 1, weak; 2, moderate; 3, strong) and extent of staining (0, 0%; 1, 1–24%; 2, 25–49%; 3, 50–74%; 4, 75–100%) were assessed. The two values were added to obtain the score sum. Cores where the tissue was lost were excluded from the analysis.

Cell culture

The human osteosarcoma cell lines MOS, U2OS, 143B, ZK58 and KPD used in this study were described previously [17,18]. Cells were grown in RPMI1640 medium supplemented with 10% fetal bovine serum, 25 U/ml penicillin and 25 µg/ml penicillin–streptomycin. All cells were cultured in a humidified incubator at 37 °C with 5% CO_2.

siRNA transfection

Transient knockdown of individual genes was achieved using siGenome SMARTpool siRNAs from Dharmacon, Thermofisher Scientific (Landsmeer, Netherlands). The final concentration of siRNA was 20 nM and this was delivered to the cells by INTERFERin siRNA transfection reagent, according to the manufacturer's procedures (Polyplus Transfection, Leusden, The Netherlands). The medium was refreshed 24 h post-transfection and transfected cells were used in experiments 48 h post-transfection. The sequences of the siRNAs targeting AVEN were *GAUUAGGGAUGCAGUUAAA*, *GAACAGGGAAAUUAUUCUA*, *UAACUGGGAUCGAUAUCAA* and *GUUAUUGGUUCGAGCCCUU*.

Cell cycle analysis

Cell-cycle analysis was performed using the Click-iT® Edu Flow Cytometry Assay Kit (Invitrogen, OR, USA). Cells were exposed to 10 µm 5-ethynyl-2-deoxyuridine (Edu) for 1 h, followed by fixation, permeabilization and staining. RNAase was added to each sample to a final concentration of 20 mg/ml. Edu was probed with Pacific blue azide and DNA was stained with FxCycle™ Far Red Stain at a final concentration of 200 nM.

Immunoblotting

Cells were lysed with SDS protein buffer (125 mM Tris–HCl, pH 6.8, 20% glycerol, 4% SDS and 0.2% bromophenol blue). Proteins were resolved by SDS–PAGE and transferred to polyvinylidine difluoride membrane. Membranes were blocked in 5% BSA–TBST (TRIS–0.05% Tween20), followed by overnight incubation with primary antibodies and 45 min incubation with HRP-conjugated secondary antibodies. Chemoluminescence was detected with a Typhoon 9400 imager (GE Healthcare).

Cell number, cell viability and real-time growth assays

Control or siRNA-transfected cells were treated with compounds for the indicated time points in black 96-well μ-Clear plates (Greiner). To determine cell numbers, cells were fixed in 4% paraformaldehyde for 15 min and nuclei were stained with Hoechst 33342 for 15 min. The plates were imaged using a BD Pathway 855 imager (Becton Dickinson). Images were processed using an Image-Pro Analyser 7.0 algorithm, yielding the number of nuclei in each well. For cell viability, cells were processed using the ATPlite One-Step Kit (Perkin-Elmer), according to the manufacturer's instructions, followed by luminescence measurement on a plate reader. For real-time cell growth analysis, the RTCA xCELLigence system (Roche Applied Sciences, Almere, The Netherlands) was used. In this system, cells are plated on a surface covered with electrodes that measures cell impedance, displayed as cell index, which is a quantitative measure of the number of cells present in the well. For the assay, the cells were seeded in an E-View 96-well plate and loaded into the RTCA station immediately. The cells were exposed to compounds 16 h later and further monitored for 72 h. Measurements were taken every 15 min.

Real-time qPCR

RNA was isolated from control or siRNA-transfected cells using RNeasy (Qiagen). cDNA was generated from 500 ng total RNA, using RNeasy Plus Kit from Qiagen. Real-time qPCR was performed in triplicate, using the SYBRGreen PCRMasterMix (Applied Biosystems) on a 7900HT fast real-time PCRsystem (Applied Biosystems). The primer sequences for CHK1 were: forward *TGGTATTGGAATAACTCACAGGGA*, reverse *TGTTCAACAAACGCTCACGA*. Data were collected and analysed using SDS2.3 software (Applied Biosystems). Relative mRNA levels after correction for *GAPDH* control mRNA were expressed using the $2^{-\Delta\Delta CT}$ method.

Three-dimensional (3D) culture assay

U2OS and MOS cells were cultured in 384-well plates (Greiner μ-Clear) in a hydrogel-containing Matrigel (Beckton–Dickinson) and collagen I, supporting invasive growth of both cell lines. Cells in culture were trypsinized and added directly to the cooled gel solution. Using a robotic liquid handler (CyBio Selma 96/60), 14.5 μl gel–cell suspension was transferred to each well of a 384-well plate (2000 cells/well). After polymerization for 30 min at 37 °C in an atmosphere of 5% CO_2, growth medium was added on top of the gel. After 3 days, when the cells had formed a network structure, compounds were diluted and added in quadruplicate wells for a period of 72 h. For measuring cell viability in 3D, 7 g/L WST-1 (Serva Electrophoresis) and 8 mg/l phenazinium methylsulphate (PMS; Sigma Aldrich) in 1× phosphate-buffered saline (PBS) were mixed in a 1:1 ratio and 5 μl was added to each well. The plates were placed at 37 °C for 5 h, after which the absorbance at 450 nM was measured, using a FluoStar plate reader. Percentage viability was thereafter calculated by robust normalization (median) of the plates between positive control (no cells; 0% viability) and negative control (solvent; 100% viability) conditions. The results are presented as mean ± SD.

For imaging, cells were fixed using 3.7% formaldehyde (Sigma-Aldrich), permeabilized with 0.1% Triton-X100 and stained for F-actin using 50 nM rhodamine–phalloidin (Sigma-Aldrich) for 12 h at 4 °C. Subsequently, the plates were washed in PBS for at least 24 h at 4 °C. The plates were then imaged on a BD Pathway 855 inverted fluorescence microscope (BD Biosciences), using a ×4 lens to capture rhodamine–phalloidin staining at focal planes spaced 50 μm throughout the gel, capturing approximately 70% of a well. Maximum intensity projections of the in-focus information of the Z-stacks were made using OcellO (OcellO BV, Leiden, The Netherlands) image analysis tools.

Synergy assessment

To assess synergy, we used the Bliss independence model, which defines that the effect of a drug at a certain concentration is independent of the presence of the other drug [19]. This model predicts the combined response C for two single compounds with effects A and B: $C = A + B - A \times B$ [20].

Statistical analysis

Dose–response curve-fitting and statistical analyses were performed using GraphPad Prism 5.0 (GraphPad Software, La Jolla, CA, USA). Unpaired two-tailed *t*-test was used to compare between groups. Significant differences between groups in the 3D assay were calculated using two-way ANOVA with Bonferroni post-test.

Results

Aven expression in human osteosarcoma samples

We used a previously published microarray dataset [15] with available follow-up data to search for mRNAs

whose expression correlated with metastasis-free survival in osteosarcoma patients. We used 53 osteosarcoma samples for which associated survival data were available. These were arranged by *Aven* mRNA expression level, and the median was used to divide the set into cases with high and low expression. The cut-off set by R2 was 218.6, with a raw p value of 0.03. Using this approach, high expression of *Aven* correlated significantly with a lower metastasis-free survival probability (Figure 1A). Next, we assessed Aven protein expression by immunohistochemistry in 31 human primary osteosarcomas and eight osteosarcoma lung metastases by immunohistochemistry. Aven protein was detected in most samples and expression was significantly higher in metastases compared to primary osteosarcoma biopsies (Figure 1B, C).

Aven silencing attenuates growth of human osteosarcoma cells

To determine Aven's role in osteosarcoma cell viability and growth, we silenced the *AVEN* gene in two human osteosarcoma cell lines, MOS and U2OS. We used a Smartpool of four siRNAs that led to a near-complete loss of Aven protein at 48 h after transfection in both cell lines (Figure 2A). In U2OS cells, transfection with this Smartpool or with any of the four individual siRNAs led to a 60–80% reduction in cell numbers as compared to control, *GAPDH*-silenced cells (Figure 2B). Likewise, MOS cells transfected with siAven showed a 60% reduction in cell numbers compared to controls (Figure 2C). Aven has been reported to suppress apoptosis in other cell types [4,5,21]. To test whether increased apoptosis was responsible for the reduced cell numbers, MOS cells transfected with siAven were treated with the pan-caspase inhibitor, z-VAD-fmk. This led to a slight increase in cell numbers but did not restore growth to cells transfected with control siRNAs (Figure 2C). The same results were obtained with U2OS: treatment with z-VAD-fmk did not restore growth of Aven-silenced cells (Figure 2D).

Aven silencing in human osteosarcoma cells triggers G_2 cell-cycle arrest

We next made use of the RTCA XCelligence system for real-time analysis of the effect of Aven silencing on human osteosarcoma cell populations. MOS cells that were MOCK (no siRNA)- or siGAPDH-transfected expanded over approximately 24 h, followed by a plateau phase after reaching confluence, whereas siAven-transfected MOS cells stopped expanding at ~18 h post-transfection (Figure 3A). Similarly, the prolonged gradual increase in cell index that was observed for U2OS cells was terminated after 18 h in response to Aven silencing. This indicated that Aven might be required for effective proliferation of osteosarcoma cells. Indeed, phosphorylation of Histone H3 Ser10, which is associated with mitosis, was attenuated in siAven-transfected MOS and U2OS cells, indicating that Aven supported cell cycle progression (Figure 3B). Furthermore, FACS analysis of MOS and U2OS cells pulsed with Edu for 1 h showed a reduction of cells in S-phase (t-test, $p < 0.05$) and a concomitant increase in G_2 (t-test, $p < 0.05$) in response to Aven silencing (Figure 3C, D).

Aven silencing attenuates ATR–Chk1 DDR signalling in human osteosarcoma cells

The role of Aven in DDR signalling has been attributed to its interaction with ATM [7]. ATM senses double-strand breaks, becomes activated and subsequently phosphorylates downstream substrates, including Chk2 and p53 [22]. We analysed ATM activation in U2OS and MOS cells treated for 4 h with 1 μM doxorubicin. Surprisingly, silencing Aven led to enhanced doxorubicin-induced ATM activation, as measured by ATM autophosphorylation at Ser1981 in MOS and U2OS cells (Figure 4A). Chk2 levels increased in response to Aven depletion in these cells (Figure 4B, C). Chk2 phosphorylation at the Thr68 ATM target site was not evident in U2OS cells, and in MOS cells doxorubicin triggered ATM Thr68 phosphorylation, irrespective of the absence or presence of Aven siRNAs (Figure 4B, C). Likewise, in MOS as well as U2OS cells, doxorubicin treatment caused strong phosphorylation of p53 at the ATM/ATR target site, Ser15, and this response was not affected by Aven silencing (Figure 4B, C).

ATR is activated in response to persistent single-stranded DNA, which is exposed at stalled replication forks and as an intermediate in several DNA damage-repair pathways [22]. Doxorubicin treatment caused increased ATR phosphorylation at Ser428 in MOS and U2OS cells, a response that was abolished by Aven silencing (Figure 4A). Moreover, phosphorylation of Chk1 at the ATR target site Ser317 after exposure to doxorubicin was also prevented in Aven-depleted MOS and U2OS cells (Figure 4B, C). This was accompanied by a loss of Chk1 protein accumulation in response to doxorubicin. The role of Aven in the accumulation and phosphorylation of Chk1 was not restricted to doxorubicin, but Aven was similarly required for this response in the context of treatment with 5 μm cisplatin or 5 μm etoposide (Figure 4D). qPCR analysis showed that changes in Chk1 protein abundance were not due to changes in mRNA (see supplementary material, Figure S2). Notably, this also excluded a reduction of Chk1 levels through off-target Aven siRNA effects.

Together, these findings indicated that Aven supports ATR–Chk1, but not ATM–Chk2 DDR signalling, in osteosarcoma cells. In contrast to ATM–Chk2 signalling, which is particularly important for the response to double-strand breaks, ATR–Chk1 signalling is also required for mitotic progression in unperturbed cells [23]. We examined whether the slightly reduced levels of Chk1 (Figure 4B–D) could underlie the cell-cycle arrest in Aven-depleted cells. In support of this, silencing

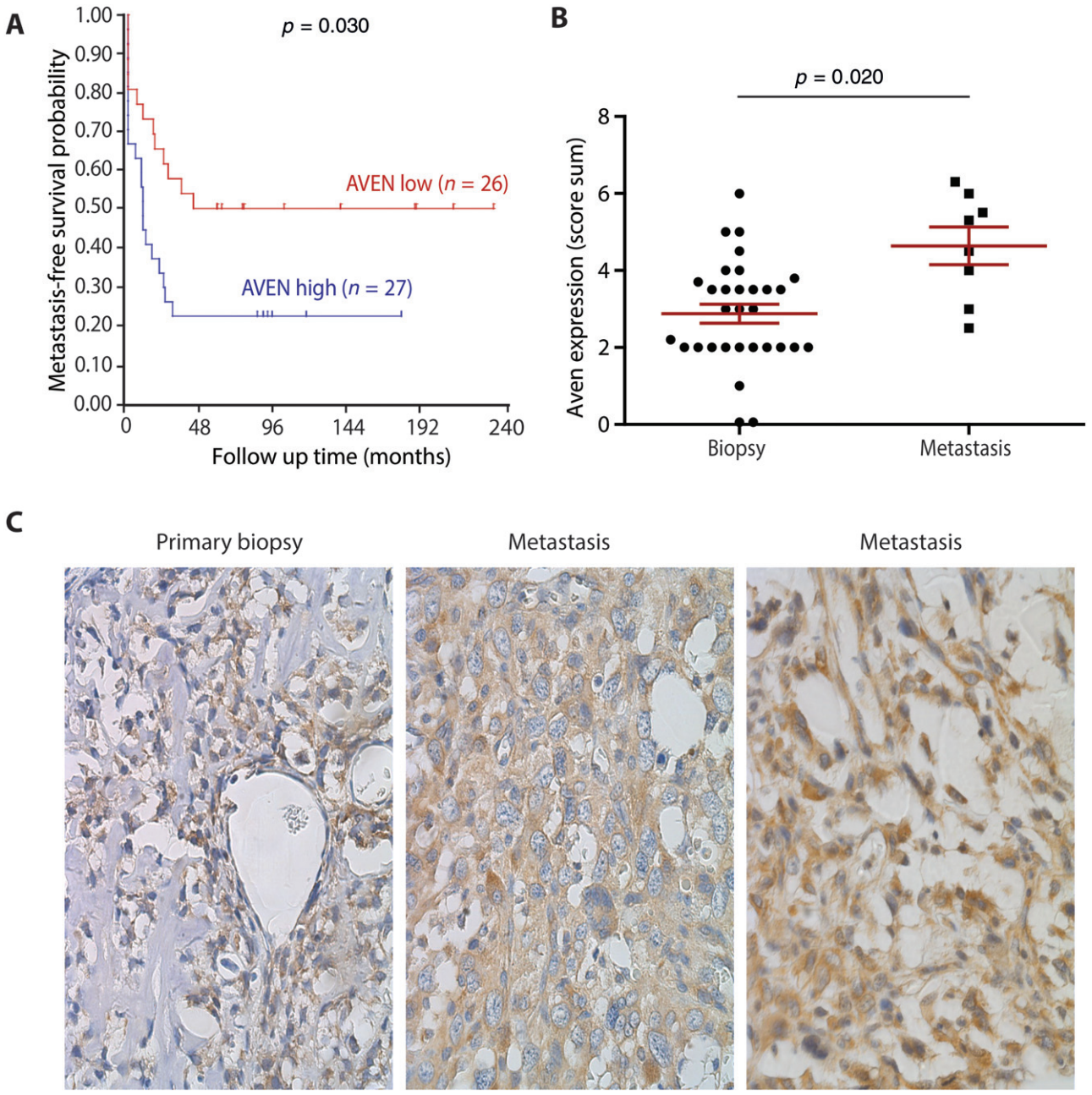

Figure 1. Aven expression in osteosarcoma biopsies. (A) Kaplan–Meier curve showing the relationship between *Aven* mRNA expression and metastasis-free survival; expression of *Aven* mRNA was analysed in 53 samples with survival data and arranged by expression; the cohort was divided into high and low expression at the median; the curve was generated using http://r2.amc.nl and *p* values were determined by Bonferroni testing. (B) Sum score of Aven expression in all tumours included in the tissue microarrays; average is shown in red; *p* values were determined by two-tailed *t*-test. (C) Representative images of Aven expression in primary osteosarcoma biopsy and metastasis; images were taken with a ×40 objective lens

Chk1, but not Chk2, impaired MOS cell growth to a similar extent as observed with Aven siRNAs (Figure 2C; see also supplementary material, Figure S3).

Pharmacological inhibition of Chk1 sensitizes osteosarcoma cells to doxorubicin

Our findings thus far suggested that Aven-controlled Chk1 signalling might represent an attractive target to sensitize osteosarcoma cells to chemotherapy. Aven inhibitors are not available, but novel Chk1/2 inhibitors that have already been tested in clinical trials are. Therefore, MOS and U2OS cells were treated with a concentration range of the Chk1/2 inhibitor, AZD7762, in combination with a concentration range of doxorubicin. Ranges were based on dose–response curves determined for each drug individually (see supplementary material, Figures S4, S5). Treatment of MOS with 25–100 nM AZD7762 by itself did not affect cell viability, but it led to strong sensitization to low (50–100 nM) concentrations of doxorubicin (Figure 5A). Calculation of the deviation from additivity, as predicted by Bliss independence [19], indicated synergy between

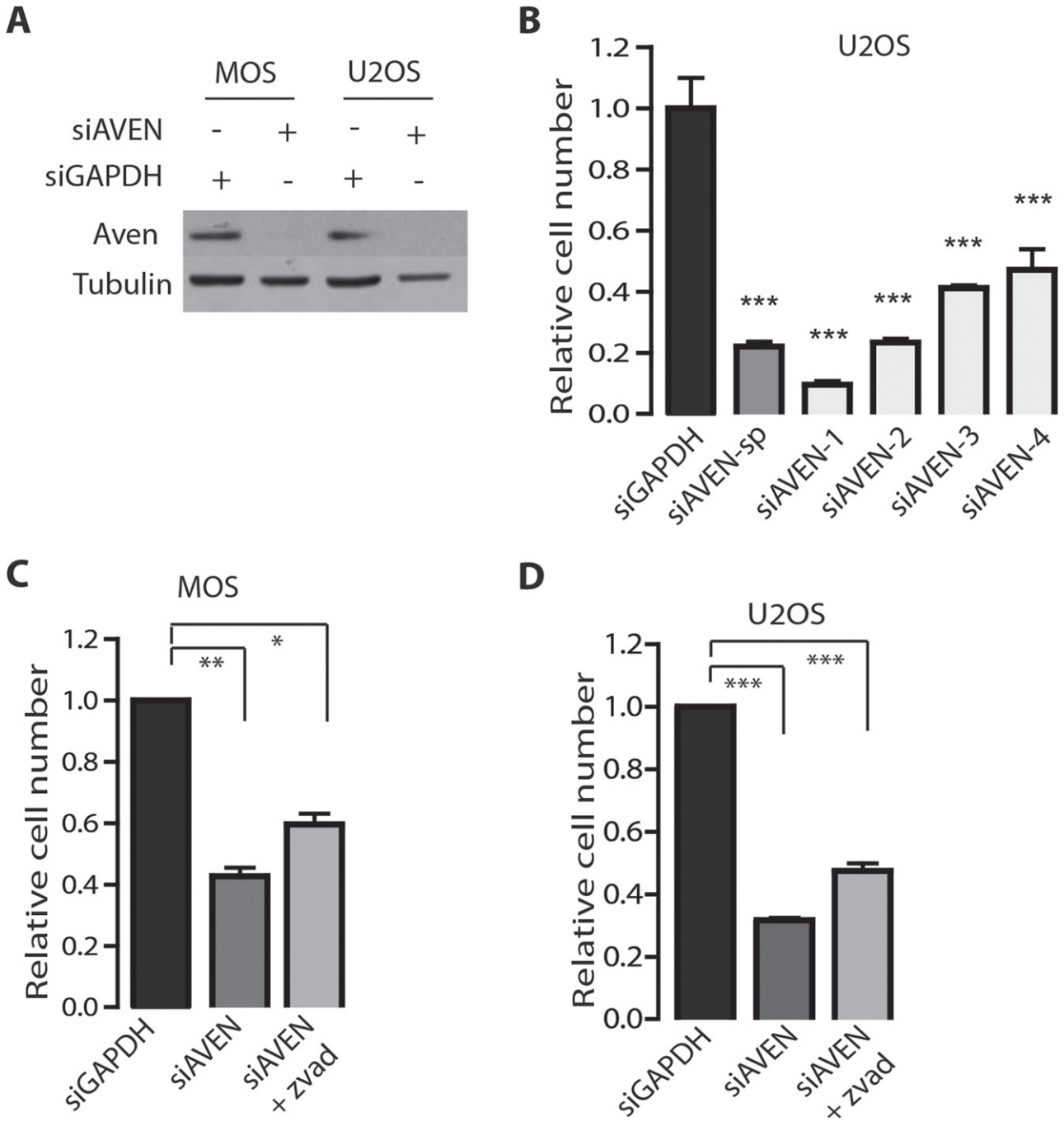

Figure 2. Effect of Aven silencing. (A) Western blot analysis of Aven protein abundance and tubulin loading control in MOS and U2OS cells transfected for 48 h with the indicated siRNA Smartpools. (B) Relative cell numbers based on Hoechst staining, 72 h post-transfection, in U2OS cells transfected with GAPDH or Aven siRNA Smartpools or with Aven single siRNAs; mean ± SD for experiments performed in quadruplicate are shown. (C, D) Relative cell numbers, based on Hoechst staining for MOS and U2OS cell lines, 72 h post-transfection, with the indicated siRNA Smartpools; cells were treated with or without z-VAD-fmk during the last 24 h (starting at 48 h post-transfection); mean ± SEM for three independent experiments performed in triplicate are shown; $^{*}p < 0.05$, $^{**}p < 0.01$, $^{***}p < 0.005$

AZD7762 and doxorubicin (Figure 5B). The same synergistic relationship between these two compounds was observed for U2OS cells (Figure 5C, D). We further explored the AZD7762–doxorubicin combination using three other human osteosarcoma cell lines, ZK58, KPD and 143B. Again, 50 nM AZD7762 slightly increased the effect of doxorubicin on ZK58 and strongly sensitized KPD and 143B cells to doxorubicin treatment (Figure 5E).

We also examined the interaction of two clinically relevant selective CHK1 inhibitors, CHIR-124 and LY2603618, with doxorubicin in osteosarcoma cells. CHIR-124 by itself already affected viability at concentrations > 25 nM, especially in U2OS cells (Figure 5F, G). At 25 nM, CHIR-124 sensitized MOS and, to a lesser extent, U2OS to doxorubicin (Figure 5F, G; see also supplementary material, Figure S6). Up to 0.25 μM LY2603618 by itself did not affect either cell

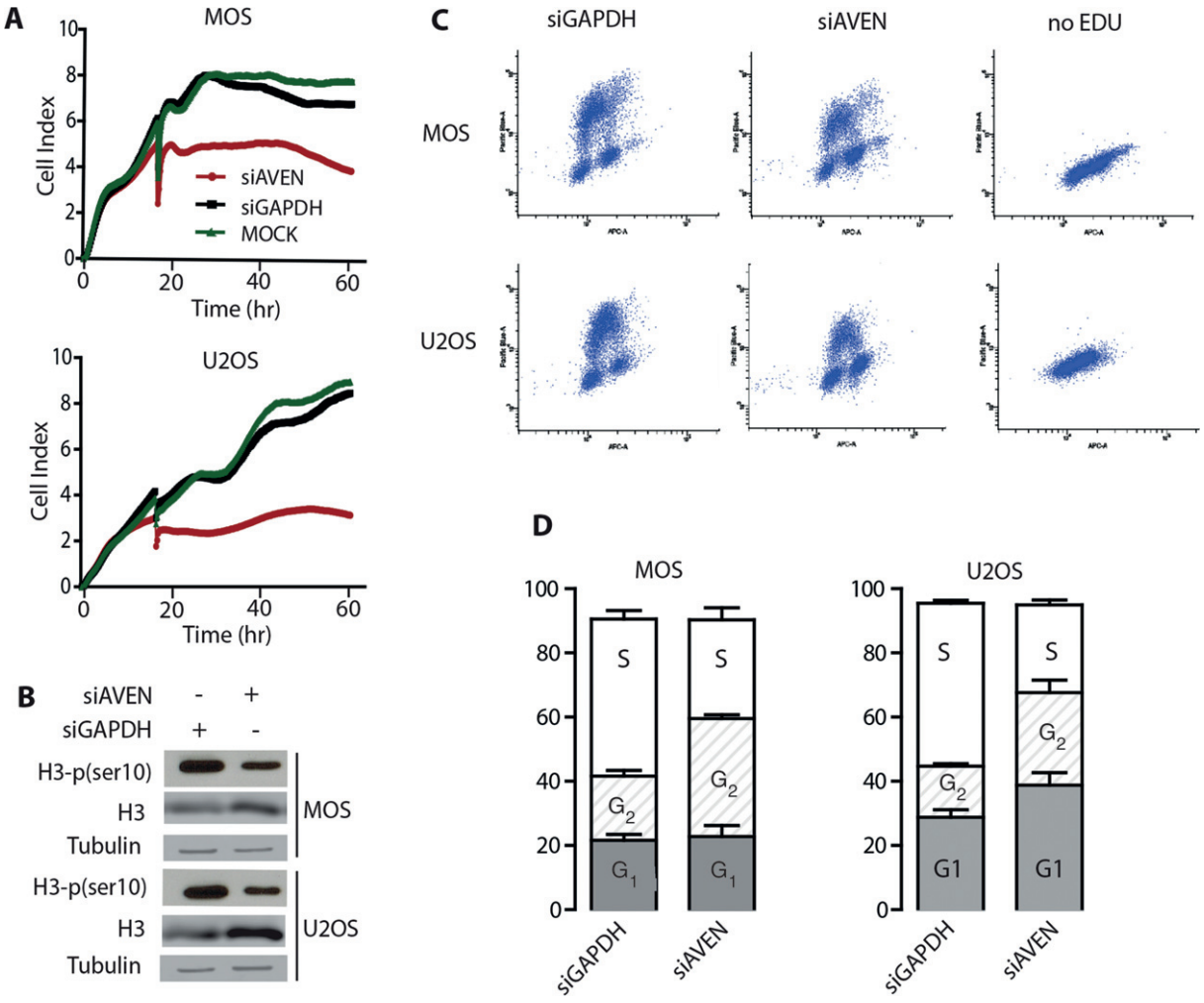

Figure 3. Aven silencing leads to cell-cycle arrest. (A) Subconfluent cultures of MOS and U2OS cells untransfected (MOCK, green) or transfected with control siGAPDH (black) or siAVEN (red) were monitored for 60 h using the RTCA Xcelligence system; the medium was refreshed at 18 h post-transfection; a representative experiment of two biological replicates, performed in quadruplicate, is shown. (B) Western blot analysis of total and phospho(Ser10) histone H3 and tubulin loading control for MOS and U2OS cells transfected with siAVEN or siGAPDH for 48 h. (C) Flow-cytometry analysis of DNA content (*x* axis) and Edu incorporation (*y* axis) in MOS and U2OS cells transfected with siAVEN or control siGAPDH pulsed for 1 h with 10 μM Edu after 48 h; a representative experiment from three biological replicates is shown. (D) Quantification of data from (C); mean and SEM of three independent experiments is shown

line, but at this concentration LY2603618 strongly augmented the effect of low concentrations of doxorubicin in U2OS and, especially, in MOS cells (Figure 5H, I; see also supplementary material, Figure S6).

Two-dimensional (2D) and 3D osteosarcoma cultures are chemosensitized by Chk1 inhibition

We confirmed chemosensitization by Chk inhibition by monitoring the cells over a period of 96 h, using the xCELLigence system. Growth of U2OS cells exposed to 0.1 μM doxorubicin was similar to growth under control conditions, whereas treatment with 0.5 μM doxorubicin caused a loss of cells (Figure 6A). Again, exposure to 50 nM AZD7762 had no effect by itself but effectively sensitized U2OS cells to 0.1 μM doxorubicin (Figure 6A).

We further validated the possibility of chemosensitization by Chk1 inhibition using 3D osteosarcoma cell cultures. MOS and U2OS cells were suspended in a mixture of collagen and matrigel and allowed to grow for 3 days. Subsequently, the cultures were exposed to a dose range of doxorubicin in the absence or presence of 50 nM AZD7762, 25 nM CHIR-124 or 0.125 μM LY2603618 for 72 h, and viability was determined using a biochemical assay. Similar to the results in 2D cultures, MOS and, to a lesser extent, U2OS were sensitized in 3D to low doses of doxorubicin when Chk1/2 was inhibited using AZD7762 (Figure 6B, C). Likewise, 3D cultures of U2OS and, especially, MOS were effectively sensitized to doxorubicin by the two selective Chk1 inhibitors CHIR-124 and LY2603618 (Figure 6B, C). Moreover, image-based analysis at the same time as biochemical viability assessment showed that combined exposure to 50 nM AZD7762 and 0.05 μM doxorubicin caused disruption of the multicellular network, which was not seen when either of these drugs was used alone (Figure 6D).

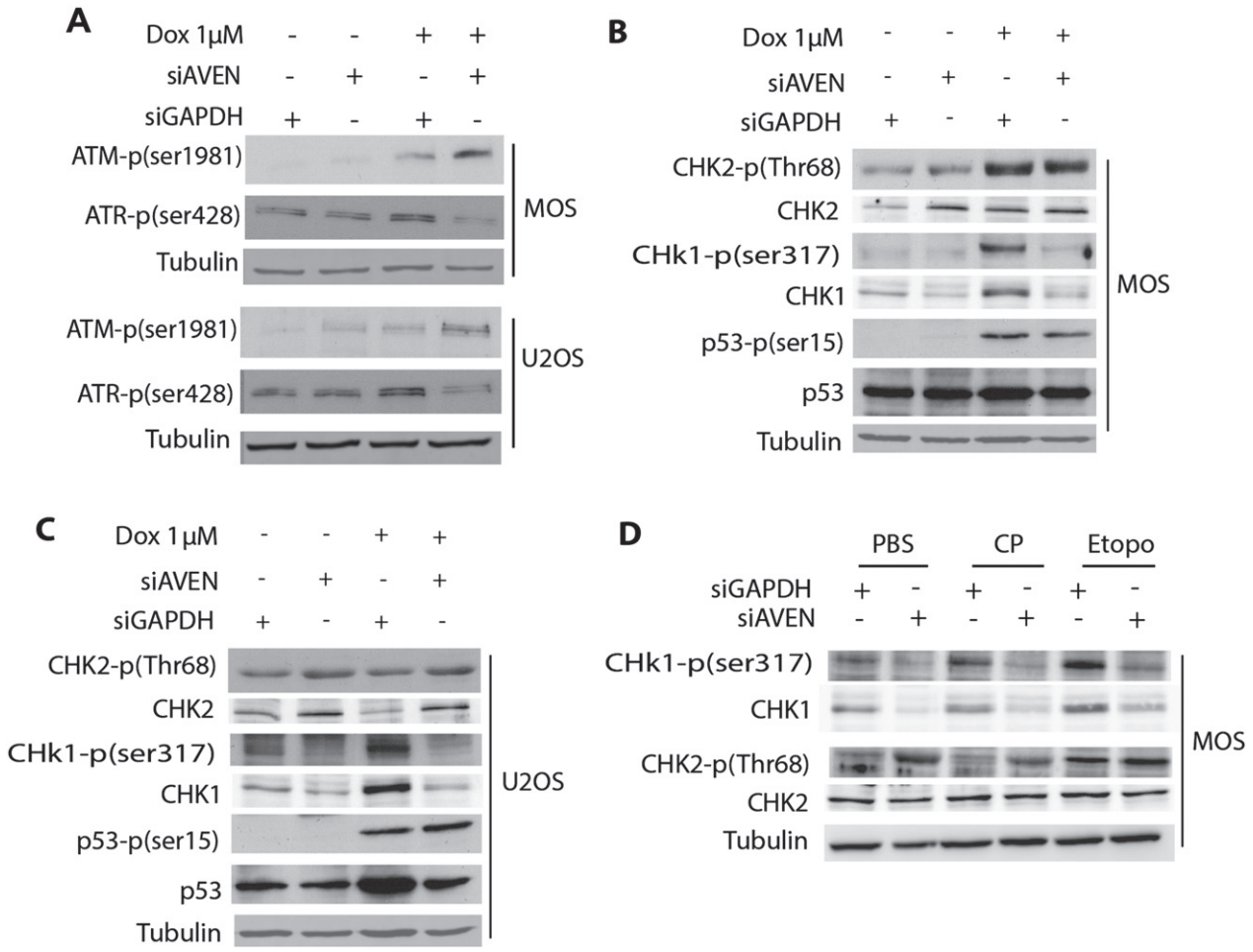

Figure 4. Aven silencing causes a shift from ATR–Chk1 to ATM–Chk2 DDR signalling. (A) Western blot analysis of total and phospho(Ser1981) ATM, total and phospho(Ser428) ATR and tubulin loading control for MOS (top) and U2OS cells (bottom), transfected for 48 h with siGAPDH or siAVEN and subsequently treated with 1 μM doxorubicin for 4 h; one representative experiment of three is shown. (B, C) Western blot analysis of total and phospho(Thr68) Chk2, total and phospho(Ser317) CHK1, total and phospho(ser15) p53 and tubulin loading control for MOS (B) and U2OS (C) cells transfected for 48 h with siGAPDH or siAVEN and subsequently treated with 1 μM doxorubicin for 4 h; one representative experiment of three is shown. (D) Western blot analysis of total and phospho(Thr68) Chk2, total and phospho(Ser317) CHK1 and tubulin loading control for MOS cells transfected for 48 h with siGAPDH or siAVEN and subsequently treated with PBS, 5 μM cisplatin (CP) or 5 μM etoposide for 4 h

Discussion

Our data point to a role for Aven in growth and therapy resistance of osteosarcomas. High expression of *Aven* mRNA correlates with low metastasis-free survival in conventional osteosarcoma patients, and Aven protein expression is high in metastasis as compared to primary biopsies of osteosarcoma. Aven has been shown to suppress apoptosis through its ability to enhance the anti-apoptotic effect of Bcl–xL and to interfere with Apaf-1-mediated apoptosome formation in leukaemic and breast cancer cells [4,5,14]. In human osteosarcoma cells, we find that depletion of Aven does not trigger cell death through apoptosis. Rather, it leads to a G_2 cell cycle arrest and, ultimately, to loss of viability by a mechanism that is not caspase-dependent. Instead, our findings indicate that this is due to impaired checkpoint kinase signalling.

Checkpoint kinases Chk1 and Chk2 coordinate progression through the cell cycle [22,24] and Chk1 is expressed in S–M phase [25]. Aven-depleted osteosarcoma cells have reduced phospho-Chk1(Ser317) and total Chk1 protein levels. Thus, Aven supports Chk1 protein synthesis or stability. As Ser317-phosphorylated Chk1 is required for DNA replication and mitotic progression [23], the important role we identify for Aven in osteosarcoma cell proliferation can be explained by its support of Chk1 abundance and phosphorylation.

The anti-apoptotic role of Aven is especially prominent in the response to genotoxic therapy. Over expression of Aven in leukaemic and breast cancer cells promotes resistance to γ-irradiation and DNA-damaging agents, such as UV, SN-38 and cisplatin [4,5]. In addition to its role in Bcl–xL function and interference with Apaf-1-mediated apoptosome formation, as discussed above, this may be related to its role in DDR signalling. Aven has been shown to support ATM activation in cycling *Xenopus* eggs and in HeLa cells treated with neocarzinostatin [7]. Remarkably, our findings demonstrate that ATM activation in response

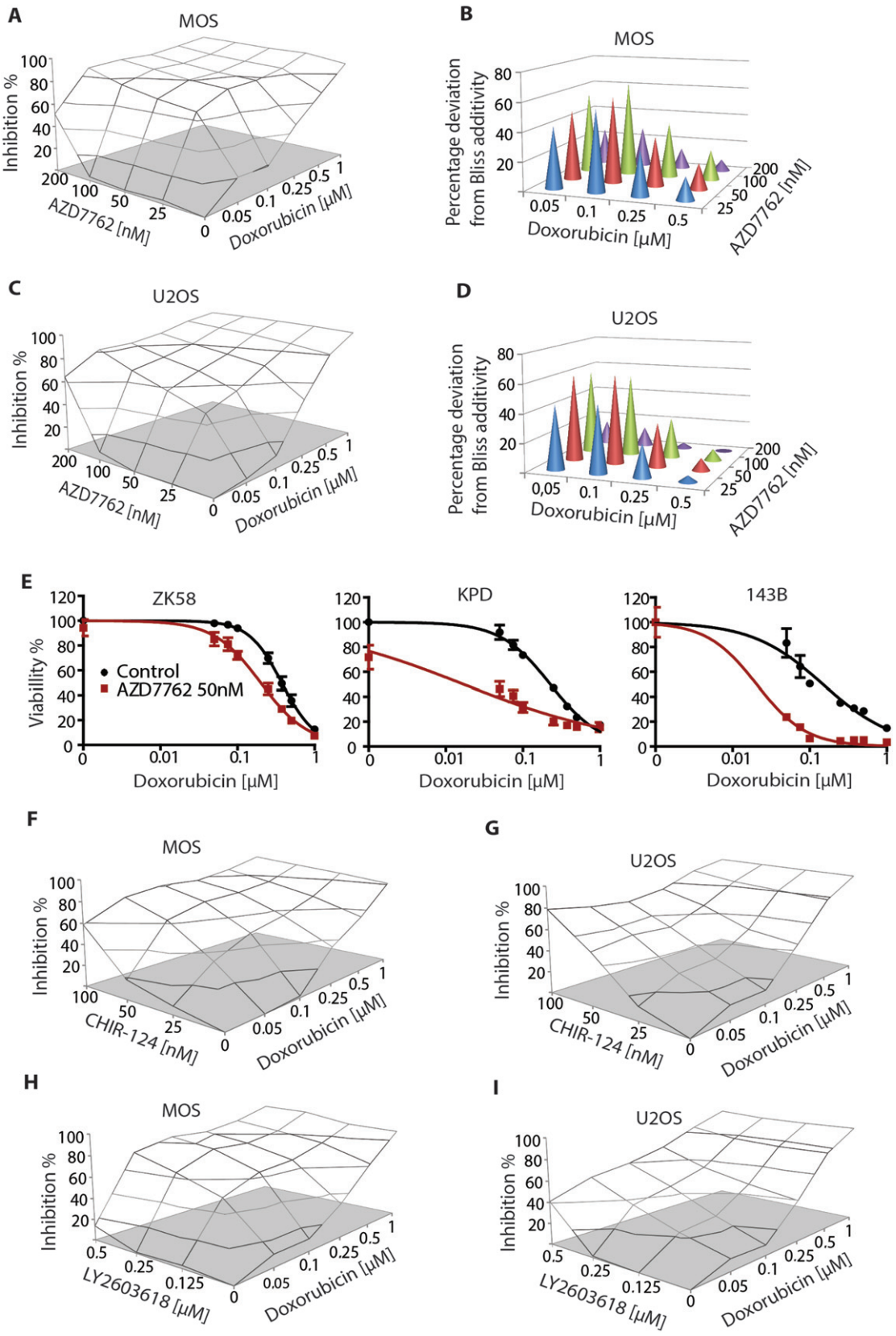

Figure 5. Treatment with Chk1 inhibitor sensitizes osteosarcoma cells to doxorubicin. (A, C) Combined effect of doxorubicin and AZD7762 dose ranges in MOS (A) and U2OS (C) cells; mean of triplicates is shown; each graph shows one representative of three independent experiments. (B, D) Needle graphs showing deviation from Bliss-predicted additivity, based on data shown in (A, C); mean of triplicates is shown; each graph shows one representative of three independent experiments. (E) Doxorubicin dose–response curves for three human osteosarcoma cell lines, as indicated, in the absence or presence of 50 nM AZD7762; cells were exposed for 72 h; each graph represents mean ± SEM. (F, G) Combined effect of doxorubicin and CHIR-124 dose ranges in MOS (F) and U2OS (G) cells; means of triplicates are shown; each graph shows one representative of three independent experiments. (H, I) Combined effect of doxorubicin and LY2603618 dose ranges in MOS (H) and U2OS (I) cells; means of triplicates are shown; each graph shows one representative of three independent experiments

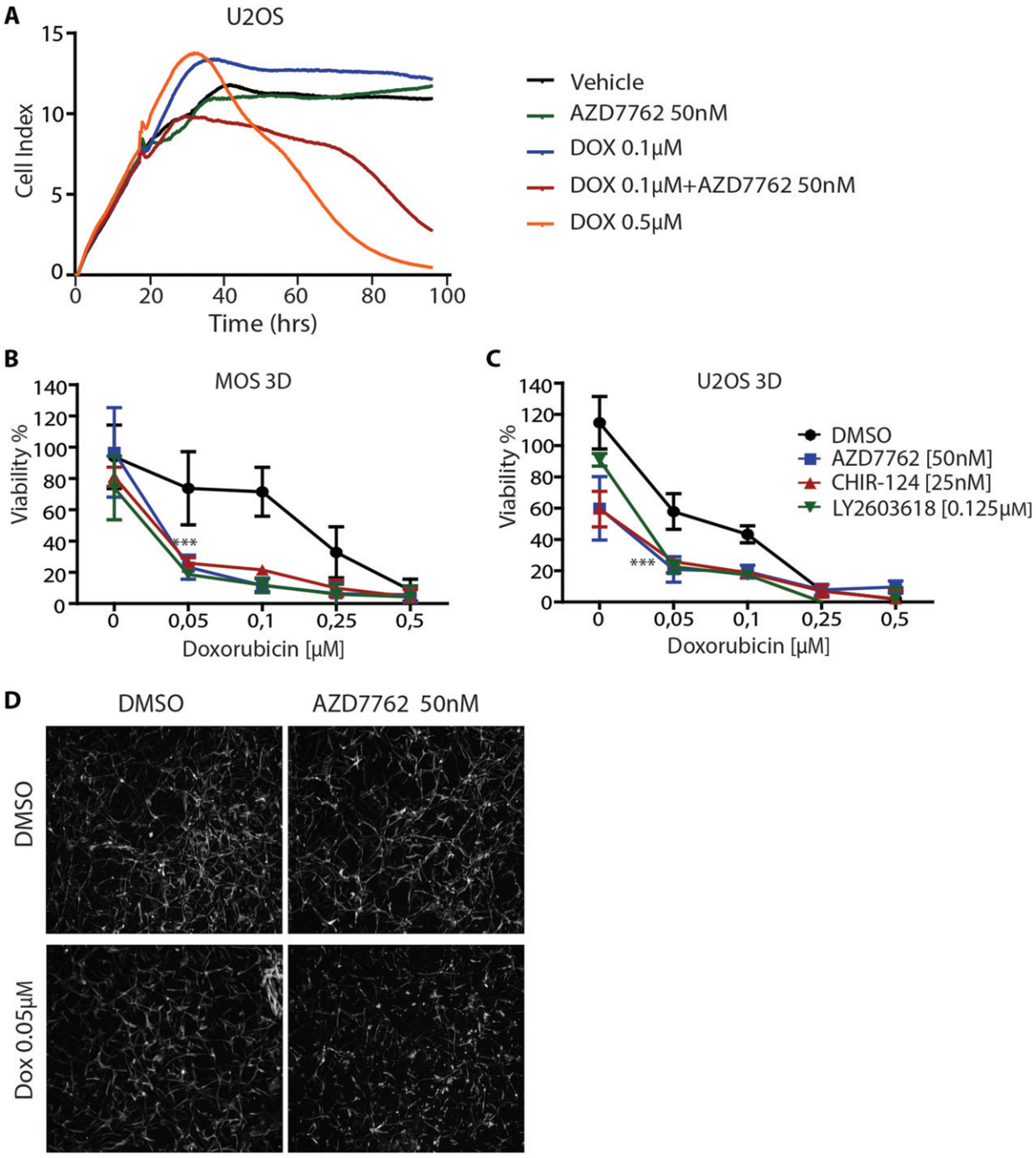

Figure 6. Osteosarcoma cells are sensitized to doxorubicin by Chk1 inhibition in 2D and 3D environments. (A) Subconfluent U2OS cultures were monitored for 90 h, using the RTCA Xcelligence system; cells were exposed 16 h after seeding to vehicle (black line), 50 nM AZD7762 (green line), 0.1 μM doxorubicin (blue line), 0.5 μM doxorubicin (orange line) or 0.1 μM doxorubicin in combination with 50 nM AZD7762 (red line); one experiment of two independent experiments performed in quadruplicate is shown. (B, C) Cell viability measured by WST assay in 3D extracellular matrix-embedded MOS (B) and U2OS (C) cultures grown for 3 days and subsequently exposed to the indicated compound concentrations for 72 h; mean ± SD of triplicates (MOS cells) or quadruplicates (U2OS cells) are shown. (D) Representative images of 3D cultures of MOS cells exposed to DMSO, 50 nM AZD7762, 0.05 μM doxorubicin or the combination of the two drugs; images are compressed Z-stacks of actin cytoskeletal staining (rhodamine–phalloidin)

to doxorubicin is fully intact, or even potentiated, in Aven-silenced osteosarcoma cells. Instead, we show that ATR activation in response to genotoxic stress is abrogated in the absence of Aven.

ATM is mainly activated by double-strand breaks, subsequently activating Chk2 to induce cell cycle arrest or apoptosis when the damage is extensive [9]. ATR is an essential regulator of genome integrity, responding to various types of DNA damage, and it activates Chk1 [8]. However, crosstalk between ATM and ATR occurs and Chk1 activation by ATR in the context of double-strand breaks is dependent on ATM [26,27]. Our data implicate Aven in ATR–Chk1 activation under conditions of genotoxic stress, whereas baseline ATR

Ser428 phosphorylation appears unaffected by Aven silencing. This suggests that Aven may facilitate the interaction between ATM and ATR, driving ATR signalling in response to double-strand breaks.

We show that, in osteosarcoma cells, the absence of Aven shifts the DDR from ATR–Chk1 to ATM–Chk2 signalling. This does not affect the activation of p53 in response to genotoxic stress. In U2OS cells, which express wild-type p53, as well as in MOS cells, which express a mutant p53, silencing Aven does not affect phosphorylation of p53 at the ATM/ATR target site Ser15 in response to doxorubicin. Under these conditions, ATM, either directly or through Chk2, likely phosphorylates p53 at Ser15 in response to DNA damage [28].

As a potential scaffold protein without enzymatic activity, Aven is unlikely to represent a candidate drug target. However, our data show that Aven-controlled Chk1 signalling may well be an interesting drug target in osteosarcoma. Depletion of Chk1, but not Chk2, to some extent phenocopies the effect of Aven silencing, and pharmacological inhibition of Chk1 at higher compound concentrations has the same effect. The use of Chk1 inhibitors for osteosarcoma appears most promising in a combination strategy. Chk1 inhibition is already used as a therapeutic approach to potentiate the efficacy of genotoxic chemotherapeutics in other cancer types [29].

The Chk1/Chk2 inhibitor, AZD7762, is known to potentiate the effect of cisplatin in ovarian clear cell carcinoma [30] as well as in multiple myeloma cells [31]. It also sensitizes pancreatic tumour cells to radiation and interferes with DNA repair in these cells [32]. However, recently it was reported that this drug would not be continued in clinical trials, due to cardiac toxicity [33]. We have tested two selective Chk1 inhibitors, CHIR-124 and LY2603618. The latter drug was tested in a phase I dose-escalation study, and acceptable safety and pharmacokinetic profiles were reported [34,35]. Here, in 2D as well as 3D cultures of human osteosarcoma cells, low concentrations of Chk1 inhibitors cause effective sensitization to low concentrations of doxorubicin.

Doxorubicin is routinely used in the treatment of osteosarcoma patients but resistance is a major obstacle [36]. Our findings indicate that abrogation of Chk1 signalling using clinically relevant drugs may be combined with chemotherapy to treat osteosarcoma more effectively. Notably, our study makes use of a panel of human osteosarcoma cell lines that are studied in culture. Future studies corroborating these findings in cell line- and patient-derived xenograft models should provide further preclinical validation that may warrant pharmacological inhibition of Aven-supported Chk1 activity in a clinical setting.

Acknowledgements

The authors would like to thank Jan Koster for help with R2, Inge Briaire-de Bruijn for immunohistochemistry and technical advice, Yvonne de Jong for designing the qPCR primers for CHK1 and Laura Heitman for her introduction to the xCELLigence system. This project was supported by a university profile grant from Leiden University/LUMC, entitled 'Translational Drug Discovery and Development'.

Author contributions

ZB performed experiments and THB carried out the 3D assay; ZB and JVMGB scored IHC experiments; ZB and EHJD conceived and analysed experiments and wrote the manuscript; and ZB, THB, AMCJ, LP, BvdW, JVMGB, PCWH and EHJD critically discussed experiments, evaluated the paper and had final approval of the submitted and published versions.

References

1. Anninga JK, Gelderblom H, Fiocco M, *et al.* Chemotherapeutic adjuvant treatment for osteosarcoma: where do we stand? *Eur J Cancer* 2011; **47:** 2431–2445.
2. Rosenberg AE, Cleton-Jansen A-M, Pinieux Gd, *et al.* Conventional osteosarcoma. In *WHO Classification of Tumours of Soft Tissue and Bone*. IARC: Lyon, 2013; 282–288.
3. Buddingh EP, Anninga JK, Versteegh MI, *et al.* Prognostic factors in pulmonary metastasized high-grade osteosarcoma. *Pediatr Blood Cancer* 2010; **54:** 216–221.
4. Chau BN, Cheng EH, Kerr DA, *et al.* Aven, a novel inhibitor of caspase activation, binds Bcl-xL and Apaf-1. *Mol Cell* 2000; **6:** 31–40.
5. Kutuk O, Temel SG, Tolunay S, *et al.* Aven blocks DNA damage-induced apoptosis by stabilising Bcl–xL. *Eur J Cancer* 2010; **46:** 2494–2505.
6. Hawley RG, Chen Y, Riz I, *et al.* An integrated bioinformatics and computational biology approach identifies new BH3-only protein candidates. *Open Biol J* 2012; **5:** 6–16.
7. Guo JY, Yamada A, Kajino T, *et al.* Aven-dependent activation of ATM following DNA damage. *Curr Biol* 2008; **18:** 933–942.
8. Mordes DA, Cortez D. Activation of ATR and related PIKKs. *Cell Cycle* 2008; **7:** 2809–2812.
9. Kurz EU, Lees-Miller SP. DNA damage-induced activation of ATM and ATM-dependent signaling pathways. *DNA Repair (Amst)* 2004; **3:** 889–900.
10. Bartek J, Lukas J. Chk1 and Chk2 kinases in checkpoint control and cancer. *Cancer Cell* 2003; **3:** 421–429.
11. Garrett MD, Collins I. Anticancer therapy with checkpoint inhibitors: what, where and when? *Trends Pharmacol Sci* 2011; **32:** 308–316.
12. Paydas S, Tanriverdi K, Yavuz S, *et al.* Survivin and aven: two distinct antiapoptotic signals in acute leukemias. *Ann Oncol* 2003; **14:** 1045–1050.
13. Choi J, Hwang YK, Sung KW, *et al.* Aven overexpression: association with poor prognosis in childhood acute lymphoblastic leukemia. *Leuk Res* 2006; **30:** 1019–1025.
14. Eissmann M, Melzer IM, Fernandez SB, *et al.* Overexpression of the anti-apoptotic protein AVEN contributes to increased malignancy in hematopoietic neoplasms. *Oncogene* 2013; **32:** 2586–2591.
15. Kuijjer ML, Rydbeck H, Kresse SH, *et al.* Identification of osteosarcoma driver genes by integrative analysis of copy number and gene expression data. *Genes Chromosomes Cancer* 2012; **51:** 696–706.
16. Mohseny AB, Szuhai K, Romeo S, *et al.* Osteosarcoma originates from mesenchymal stem cells in consequence of aneuploidization and genomic loss of Cdkn2. *J Pathol* 2009; **219:** 294–305.

17. Mohseny AB, Machado I, Cai Y, *et al.* Functional characterization of osteosarcoma cell lines provides representative models to study the human disease. *Lab Invest* 2011; **91:** 1195–1205.
18. Ottaviano L, Schaefer KL, Gajewski M, *et al.* Molecular characterization of commonly used cell lines for bone tumor research: a trans-European EuroBoNet effort. *Genes Chromosomes Cancer* 2010; **49:** 40–51.
19. Greco WR, Bravo G, Parsons JC. The search for synergy: a critical review from a response surface perspective. *Pharmacol Rev* 1995; **47:** 331–385.
20. Borisy AA, Elliott PJ, Hurst NW, *et al.* Systematic discovery of multicomponent therapeutics. *Proc Natl Acad Sci USA* 2003; **100:** 7977–7982.
21. Figueroa B, Jr., Chen S, Oyler GA, *et al.* Aven and Bcl–xL enhance protection against apoptosis for mammalian cells exposed to various culture conditions. *Biotechnol Bioeng* 2004; **85:** 589–600.
22. Kastan MB, Bartek J. Cell-cycle checkpoints and cancer. *Nature* 2004; **432:** 316–323.
23. Wilsker D, Petermann E, Helleday T, *et al.* Essential function of Chk1 can be uncoupled from DNA damage checkpoint and replication control. *Proc Natl Acad Sci USA* 2008; **105:** 20752–20757.
24. Bartek J, Falck J, Lukas J. CHK2 kinase – a busy messenger. *Nat Rev Mol Cell Biol* 2001; **2:** 877–886.
25. Kaneko YS, Watanabe N, Morisaki H, *et al.* Cell-cycle-dependent and ATM-independent expression of human Chk1 kinase. *Oncogene* 1999; **18:** 3673–3681.
26. Jazayeri A, Falck J, Lukas C, *et al.* ATM- and cell cycle-dependent regulation of ATR in response to DNA double-strand breaks. *Nat Cell Biol* 2006; **8:** 37–45.
27. Cuadrado M, Martinez-Pastor B, Murga M, *et al.* ATM regulates ATR chromatin loading in response to DNA double-strand breaks. *J Exp Med* 2006; **203:** 297–303.
28. Harper JW, Elledge SJ. The DNA damage response: ten years after. *Mol Cell* 2007; **28:** 739–745.
29. McNeely S, Beckmann R, Bence Lin AK. CHEK again: revisiting the development of CHK1 inhibitors for cancer therapy. *Pharmacol Ther* 2014; **142:** 1–10.
30. Itamochi H, Nishimura M, Oumi N, *et al.* Checkpoint kinase inhibitor AZD7762 overcomes cisplatin resistance in clear cell carcinoma of the ovary. *Int J Gynecol Cancer* 2014; **24:** 61–69.
31. Landau HJ, McNeely SC, Nair JS, *et al.* The checkpoint kinase inhibitor AZD7762 potentiates chemotherapy-induced apoptosis of p53-mutated multiple myeloma cells. *Mol Cancer Ther* 2012; **11:** 1781–1788.
32. Morgan MA, Parsels LA, Zhao L, *et al.* Mechanism of radiosensitization by the Chk1/2 inhibitor AZD7762 involves abrogation of the G_2 checkpoint and inhibition of homologous recombinational DNA repair. *Cancer Res* 2010; **70:** 4972–4981.
33. Sausville E, Lorusso P, Carducci M, *et al.* Phase I dose–escalation study of AZD7762, a checkpoint kinase inhibitor, in combination with gemcitabine in US patients with advanced solid tumors. *Cancer Chemother Pharmacol* 2014; **73:** 539–549.
34. Weiss GJ, Donehower RC, Iyengar T, *et al.* Phase I dose–escalation study to examine the safety and tolerability of LY2603618, a checkpoint 1 kinase inhibitor, administered 1 day after pemetrexed 500 mg/m^2 every 21 days in patients with cancer. *Invest New Drugs* 2013; **31:** 136–144.
35. Calvo E, Chen VJ, Marshall M, *et al.* Preclinical analyses and phase I evaluation of LY2603618 administered in combination with Pemetrexed and cisplatin in patients with advanced cancer. *Invest New Drugs* 2014; **5:** 955–968.
36. Luetke A, Meyers PA, Lewis I, *et al.* Osteosarcoma treatment – where do we stand? A state of the art review. *Cancer Treat Rev* 2014; **40:** 523–532.

SUPPLEMENTARY MATERIAL ON THE INTERNET

The following supplementary material may be found in the online version of this article:

Figure S1. Immunohistochemistry with or without primary Aven antibody on control testis tissue

Figure S2. qPCR analysis showing *Chk1* mRNA levels in U2OS cells transfected for 48 h with the indicated siRNAs

Figure S3. MOS cells were transfected with siGAPDH, siChk1, siChk2 for 72 h and cell numbers were determined by Hoechst staining and counting of nuclei

Figure S4. Dose–response curve of doxorubicin in MOS and U2OS cells

Figure S5. Dose–response curve of AZD7762 in MOS and U2OS cells

Figure S6. Needle graphs showing deviation from Bliss-predicted additivity in MOS and U2OS cells exposed to doxorubicin and CHIR-124 or doxorubicin and LY2603618 dose ranges